Appl Phys B (2012) 107:459–467
DOI 10.1007/s00340-012-4908-x

Applied Physics B
Lasers and Optics

Compact QEPAS sensor for trace methane and ammonia detection in impure hydrogen

L. Dong · J. Wright · B. Peters · B.A. Ferguson · F.K. Tittel · S. McWhorter

Received: 5 December 2011 / Published online: 12 May 2012

Abstract A compact two-gas sensor based on quartz-enhanced photoacoustic spectroscopy (QEPAS) was developed for trace methane and ammonia quantification in impure hydrogen. The sensor is equipped with a micro-resonator to confine the sound wave and enhance QEPAS signal. The normalized noise-equivalent absorption coefficients (1σ) of 2.45×10^{-8} cm^{-1} W/$\sqrt{}$Hz and 9.1×10^{-9} cm^{-1} W/$\sqrt{}$Hz for CH_4 detection at 200 Torr and NH_3 detection at 50 Torr were demonstrated with the QEPAS sensor configuration, respectively. The influence of water vapor on the CH_4 channel was also investigated.

1 Introduction

The development of robust and compact optical sensors for muti-gas detection is of considerable interest in diverse applications, such as gas purity measurements, industrial processing control, environmental monitoring and medical diagnostics. Quartz-enhanced photoacoustic spectroscopy (QEPAS) is a rapidly developing, sensitive, selective spectroscopic technique for laser-based trace gas detection with a fast response time [1, 2]. QEPAS combines the main characteristics of photoacoustic spectroscopy (PAS) with the benefits of using a quartz tuning fork (QTF), thus providing an ultra-compact, cost-effective, robust acoustic detection module (ADM). Moreover, QEPAS can achieve sensitivities comparable to conventional PAS, but with reduced ambient acoustic noise due to the acoustic quadrupole nature of the QTF [3].

The micro-resonator (mR) plays a crucial role in QEPAS sensors and acts similarly to the acoustic resonator in conventional PAS [4]. In the QEPAS sensor architecture, the mR consists of two rigid hypodermic tubes that surround the QTF. The energy of the acoustic wave induced by radiation excitation is accumulated in the mR by means of the resonant effect and subsequently transferred to the QTF as the result of coupling between the mR and QTF. Recent studies reported that the optimal length of each mR tube is between $\lambda_s/4$ and $\lambda_s/2$ where λ_s is the wavelength of sound [3, 5]. The results reported in Ref. [3] showed that an optimized mR configuration can further improve the QEPAS signal-to-noise ratio (SNR) by up to 30 times, as compared to using a bare QTF.

To date, the QEPAS sensor technique has been employed to detect, monitor and quantify several molecules with well resolved rotational-vibrational lines in the near-infrared spectral range (e.g., NH_3, CO_2, CO, HCN, HCl, H_2O, H_2S, CH_4, C_2H_2, C_2H_4) [6–10] as well as in the mid-infrared spectral region (e.g., NO, N_2O, CO, NH_3, C_2H_6, and CH_2O) [11–16]. QEPAS has also been demonstrated with larger molecules with broad, unresolved absorption spectra, such as ethanol, acetone and Freon [17]. However, QEPAS-based sensors reported above were primarily developed for monitoring target gas concentrations for N_2 or air as the carrier gas. In this work we report the design, development and optimization of a compact trace methane (CH_4) and ammonia (NH_3) QEPAS-based sensor platform if impure H_2 is the carrier gas. Detection and quantitative measurement of trace impurities including CH_4 and NH_3 in hydrogen gas process streams is of critical importance to re-

L. Dong · F.K. Tittel (✉)
Department of Electrical and Computer Engineering, Rice University, 6100 Main Street, Houston TX 77005, USA
e-mail: FKT@rice.edu

J. Wright · B. Peters · B.A. Ferguson · S. McWhorter
Hydrogen Technology Research Laboratory, Savannah River National Laboratory, Aiken, SC 29808, USA

finement and purification of hydrogen isotopologues at the Savannah River National Laboratory (SRNL), Aiken, SC. The QEPAS technique presents a unique, new methodology for impurity analysis within impure hydrogen gas streams. The reported speed of sound in hydrogen is 1330 m/s at room temperature [18] which is ∼4 times faster than in air, since the density of H_2 is only 1/14 of the density of air. The parameters and the performance of mR are strongly dependent on the properties of the carrier gas, in particular the gas density, speed of sound within the gas. Thus, the mR used in N_2 or air is no longer optimized when H_2 is the carrier gas. The mR parameters must be reoptimized in order to meet the requirement of the H_2 carrier gas environment. Furthermore, the QEPAS sensor detection sensitivity can be affected by the conversion efficiency of the absorbed optical radiation power into the sound energy, which is determined by the vibrational-to-translational (V-T) energy transfer rate of the target gas. This rate usually changes with different carrier gases and in the presence of H_2O vapor, which is an efficient catalyst for the vibrational energy transfer reactions in the gas phase. We also performed a side-by-side inter-comparison between the new QEPAS sensor and the previously reported QEPAS sensor designed for detecting trace CH_4 and NH_3 in H_2 and in N_2 carriers, respectively.

2 Sensor design

The diode laser based QEPAS sensors employ commercially available QTFs that are designed for use as the frequency reference at a resonant frequency of ∼32.8 kHz. The speed of sound at room temperature in air is ∼340 m/s [18]. Based on Ref. [3, 5], the empirically determined optimal mR tube length was 4.4 mm in N_2, which is between $\lambda_s/4$ and $\lambda_s/2$, as mentioned above. The optimal mR tube inner diameter was ∼0.5 mm. However, with hydrogen as the carrier gas, the estimated optimal mR tube length was ∼20 mm due to the fast speed of sound. Thus, the total length of the two mR tubes employed in one ADM for the sensor platforms increased to ∼40 mm. This increased mR length represents a challenge to focus the excitation diode laser beam passing through the 40-mm-long mR and the 300-μm gap between the prongs of the QTF without optical contact. In fact, any optical contact between the diode laser excitation radiation and the mR or QTF results in an undesirable, non-zero background, which can be more than ten times larger than the thermal noise level of QEPAS [12]. As a result, the ∼20-mm optimized mR tube length (which must be matched to the acoustic wavelength so that the acoustic energy can be efficiently accumulated in the mR tube) is no longer suitable for QEPAS-based trace gas detection in H_2.

In previous QEPAS-based sensor studies it was observed that a non-matched length short mR can still increase the QEPAS sensitivity by a factor of 10 times or more [2, 16]. In this case, the mR tubes act to confine the sound wave, but do not exhibit a well defined resonant behavior. Therefore we adopted a non-matched mR configuration for the QEPAS-based sensor used to detect trace gases in a H_2 carrier gas. Two 5-mm-long mR tubes, whose length is 4 times smaller than the evaluated 20-mm optimal length, were employed. The mR tubes featured an inner tube diameter of 0.58 mm and outer tube diameter of 0.9 mm.

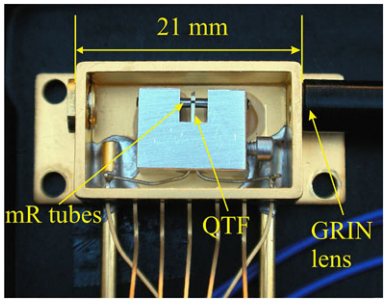

Fig. 1 Fiber-coupled QEPAS acoustic detection module (ADM)

A typical acoustic detection module (ADM) for a QEPAS-based sensor incorporates a QTF, mR tubes, and an enclosure that allows operation at a reduced pressure determined for the targeted trace gas mixture. A fiber-coupled ADM was used in the sensor, depicted in Fig. 1. This ADM was assembled in a telecom-style butterfly package by Achray Photonics, Inc. The near-infrared radiation was delivered to the ADM via a single-mode optical fiber and then focused by a GRIN lens. Active optical alignment was used to ensure free propagation of the radiation through the mR tubes. Epoxy was used to attach both the QTF and the mR tubes to the metallic mount.

The QEPAS sensor system shown in Fig. 2 consists of three parts: a control electronics unit (CEU) [1], an ADM, and a switching module. The diode laser for NH_3 detection (JDS Uniphase, CQF 935.908-19570) and two reference cells (Wavelength References, Inc.) for CH_4 and NH_3 monitoring were mounted inside the CEU. An electronic switchboard to select the appropriate signal from one of the two reference cells was also incorporated into the CEU. The CEU was responsible for measuring the basic QTF parameters (the resonant frequency f_0, quality factor Q and resistance R of the QTF), modulating the two diode lasers at half the resonant frequency of the QTF frequency for optimal detection sensitivity, and locking of the laser wavelength to a selected absorption line of the target analyte. To determine the QTF parameters, a sine wave excitation voltage was applied to the QTF electrodes, and the excitation frequency was scanned to determine the QTF resonant frequency by measuring the QTF current. The Q factor was derived from the QTF ring-down time following a rapid interruption of the excitation voltage. The diode laser for CH_4

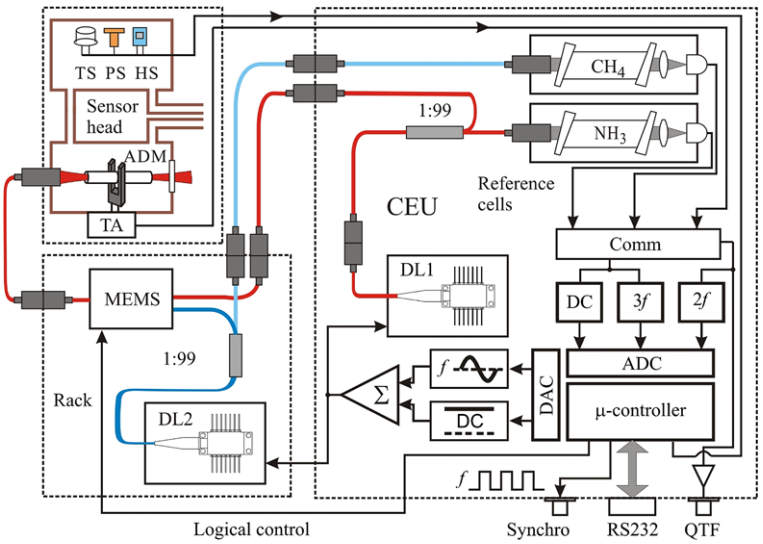

Fig. 2 Schematic of a compact two-gas QEPAS sensor. *TS*, *PS*, *HS*—temperature, pressure, and humidity sensors, *ADM*—acoustic detection module, *TA*—transimpedance amplifier, *DL*1, *DL*2—diode lasers, *CEU*—control electronics unit

detection (NEL, NLK1U5FAAA) and a 4 × 4 MEMs optical switch were mounted in the switching module. The 4 × 4 MEMS switch was realized by combining two 1 × 4 switches (LightBand Mini 1 × 4, Agiltron, Inc.). The MEMs switch was controlled to direct either of the two diode lasers to the ADM via a parallel 4-bit binary code provided by the CEU. The QEPAS-based sensor head consisted of the ADM and a compact enclosure in which ultra small temperature, pressure and humidity sensors were mounted. Finally, a notebook PC computer communicated with the CEU via a RS232 serial port for collection of $2f$ harmonic data and gas temperature, humidity, pressure parameters.

3 Signal amplitude and noise sources of QEPAS

The QEPAS signal S_{QEPAS} can be expressed as [19]

$$S_{\mathrm{QEPAS}} = C_{\mathrm{ADM}} P_0 C Q(p)\alpha(p)\varepsilon(p), \tag{1}$$

where C_{ADM} is the ADM constant, P_0 is the incident optical power, C the detected gas concentration, Q the quality factor of the QTF, α the peak intensity of the $2f$ absorption spectrum, and ε is the conversion efficiency of the absorbed optical radiation power into acoustic energy. Q, α, and ε are pressure dependent. In addition, the peak intensity α depends on the laser wavelength modulation (WM) depth. When the modulation width is close to the absorption linewidth, the maximum $2f$ signal is achieved. Therefore in order to optimize the sensor performance, both the gas pressure and the WM depth must be appropriately selected.

Assuming only collision deexcitation between molecules is taken into account, it is known that the conversion efficiency is related to the relaxation time τ of a target gas as follows [20, 21]:

$$\varepsilon(p) = \frac{1}{\sqrt{1+\tan^2\theta}}, \tag{2}$$

$$\tan\theta = 2\pi f \tau(p), \tag{3}$$

$$\tau(p) = \frac{P_0\tau_0}{p}, \tag{4}$$

where θ is the QEPAS signal phase, f is the modulation frequency of the optical excitation, and $P_0\tau_0$ is the relaxation time constant. These equations imply that increasing pressure leads to a corresponding increased rate of molecular collisions and produces a faster V-T relaxation of the target analyte.

A background noise analysis of a QEPAS-equivalent circuit shows that two primary noise sources are the thermal noise associated with mechanical dissipation in the QTF, as represented by the R in the series RLC-equivalent circuit [1]:

$$\sqrt{\langle V_{N-R}^2\rangle} = R_{\mathrm{g}}\sqrt{\frac{4k_{\mathrm{B}}T}{R}}\sqrt{\Delta f}, \tag{5}$$

$$R = \frac{1}{Q}\sqrt{\frac{L}{C}}, \tag{6}$$

and the thermal noise of the feedback resistor:

$$\sqrt{\langle V_{N-R_{\mathrm{g}}}^2\rangle} = \sqrt{4k_{\mathrm{B}}TR_{\mathrm{g}}}\sqrt{\Delta f}, \tag{7}$$

where $R_{\mathrm{g}} = 10$ MΩ is the feedback resistor of transimpedance preamplifier, k_{B} is the Boltzmann constant, T is QTF temperature, and Δf is the detection bandwidth. As the noise caused by feedback resistor R_{g} is $(R_{\mathrm{g}}/R)^{1/2}$ times lower than the QTF noise, R_{g} is usually neglected over typical values of R (10 to 200 kΩ). Additionally, it has been

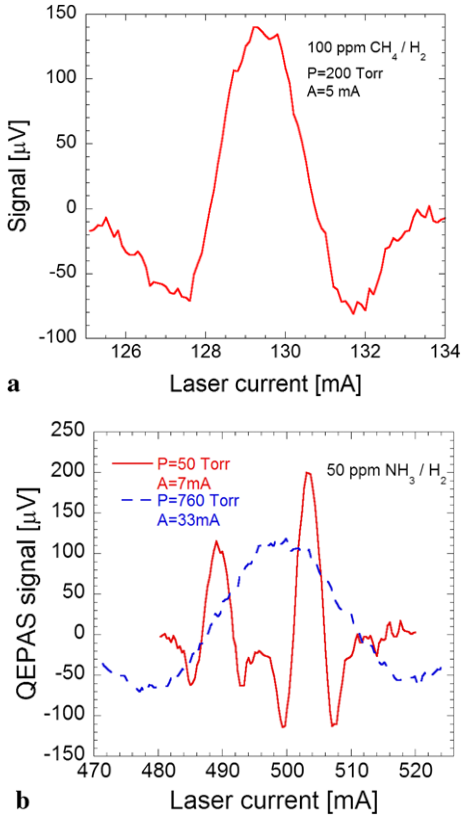

Fig. 3 (**a**) QEPAS spectra of the CH_4 lines acquired at a 100-ppmv CH_4 concentration and 200-Torr H_2. (Modulation amplitude: $A = 5$ mA, detection bandwidth: $\Delta f = 0.785$ Hz). (**b**) QEPAS spectra of the NH_3 lines for a 50-ppmv NH_3 concentration acquired at 50 Torr and 760 Torr H_2, respectively. ($A = 7$ mA for 50 Torr, $A = 33$ mA for 760 Torr, $\Delta f = 0.785$ Hz)

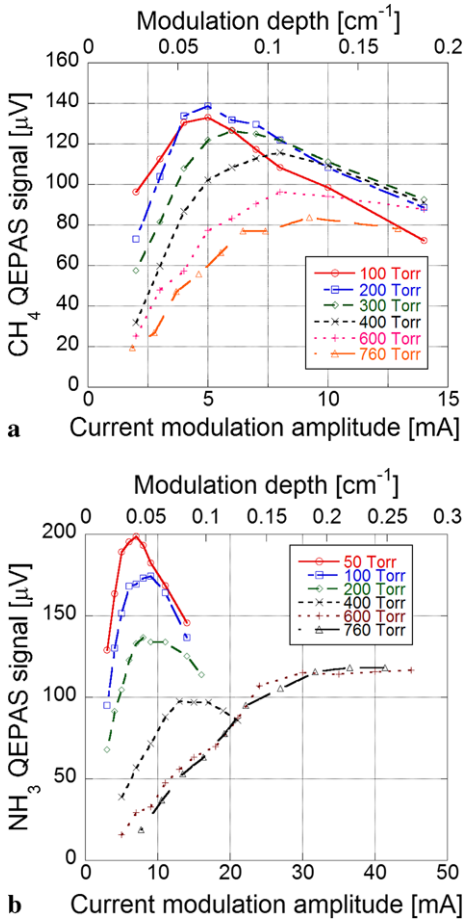

Fig. 4 (**a**) QEPAS signal corresponding to the peak CH_4 absorption near 6057.1 cm^{-1} as functions of WM depth and current modulation amplitude acquired at different pressures. (**b**) QEPAS signal corresponding to the peak NH_3 absorption near 6528.76 cm^{-1} as functions of WM depth and current modulation amplitude acquired at different pressures

verified in previous QEPAS performance tests that the observed QEPAS noise is equal to the theoretical noise of the QTF [4, 11, 19].

4 Optimization and sensitivity of the CH_4 detection channel

The R(4) manifold of the CH_4 $2\nu_3$ band near 6057.1 cm^{-1} was employed as the selected CH_4 detection line. The R(4) manifold consists of four discrete absorption lines. An example of the QEPAS spectra acquired for using 100 ppm CH_4 at 200 Torr H_2 mixture is shown in Fig. 3(a). The four discrete absorption lines are closely spaced so that only one merged line was observed resulting in slight asymmetry at 200 Torr. Due to the absence of the CH_4 broadening coefficient in H_2, it is difficult to obtain the optimal laser WM amplitude for different pressures by numerically simulating the $2f$ line shapes based on the approach described in Ref. [19]. Optimization of the gas pressure and the WM depth was carried out experimentally with a 100 ppm (by volume) CH_4 in H_2 mixture. The flow rate was set to 150 sccm.

The CH_4 QEPAS $2f$ signal corresponding to the peak absorption was plotted as a function of gas pressure and laser current modulation depth as shown in Fig. 4(a). Maximum signal was observed at 200 Torr. The measured Q factors and the R values of the QTF are shown in Fig. 5 (dashed lines). The Q factor of a QTF is dependent on the QTF temperature, the surrounding gas pressure, and the property of the major chemical composition of the target analyte. Due to the smaller vibrational damping in H_2 (as compared to N_2), the QTF has a high Q factor (>30,000). The high QTF Q factor enhances the QEPAS signal amplitude since the QEPAS signal is proportional to the Q factor (1). However, based on (6), the product of Q and R of the QTF is a constant because the equivalent QTF L and C parameters are constant. As a result, the higher Q factor decreases R, resulting in higher noise contribution. For comparison, at 200 Torr, the noise level (1σ) is 4.8 μV in hydrogen, while it is only 2.7 μV in nitrogen. So in order to appropriately optimize and assess the CH_4 channel performance, both sig-

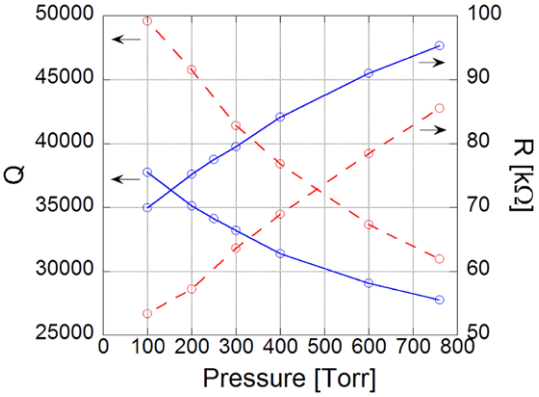

Fig. 5 *Dashed lines*: measured Q factor and R values in dry H_2 as a function of pressures. *Solid lines*: measured Q factor and R values in H_2 with 2.29% H_2O vapor at different gas pressures

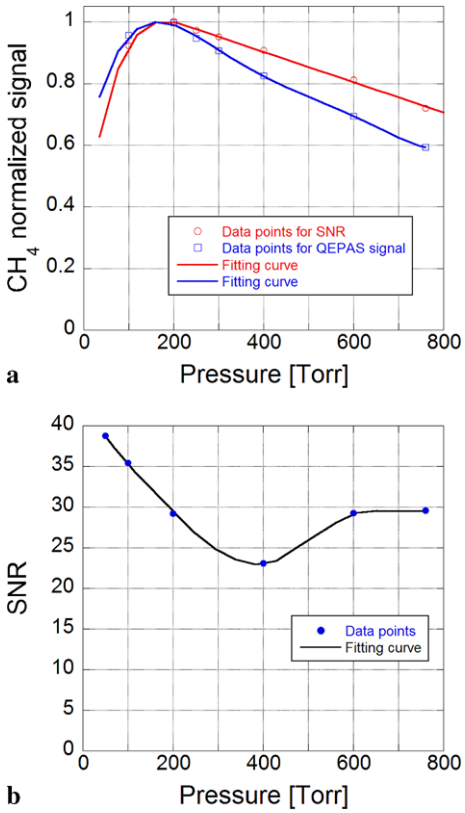

Fig. 6 (**a**) Plot of the QEPAS maximum signal amplitude and signal–to-noise ratio of CH_4 as a function of pressure. Each curve is normalized to its maximum value. (**b**) SNR with optimal laser current modulation amplitude for a 50-ppmv NH_3 in H_2 mixture and a 1-s averaging time

nal and noise should be considered. In Fig. 6(a), the normalized maximum signal amplitude and signal-to-noise ratio (SNR) are plotted as a function of pressure, based on the data in Fig. 4(a) and (5). The optimal detection pressure for both the CH_4 QEPAS signal amplitude and the SNR occur at ∼200 Torr. Unlike CH_4 trace detection in nitrogen [19],

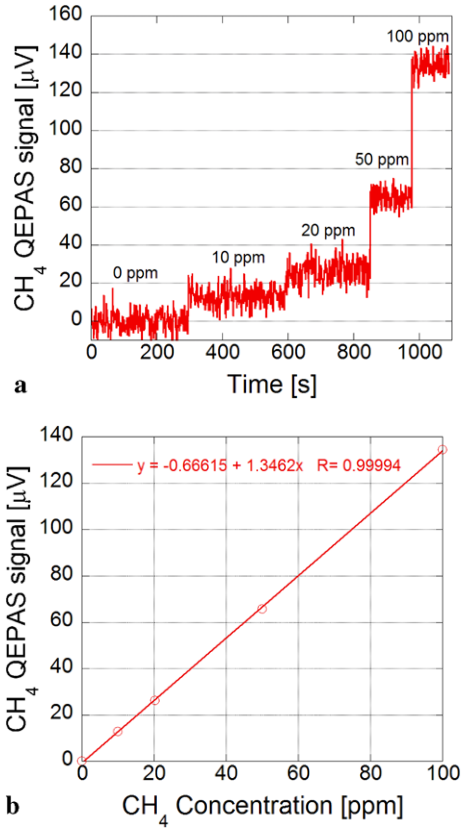

Fig. 7 (**a**) QEPAS signal repetitively recorded while the CH_4 concentration was varied by changing gas cylinders with different calibrated CH_4 concentrations. (**b**) Same data averaged and plotted as a function of certified concentration of CH_4 gas cylinders

the pressure shift for the two optimal detection pressures is not observed. This pressure behavior is due to insensitivity of R to pressure changes in hydrogen. Between 100 to 760 Torr, the R values range from 100 to 230 kΩ in nitrogen, while the R values range from 53 to 86 kΩ in hydrogen. Using (5), smaller values of R result in a smaller variation of noise level in hydrogen than in N_2. Consequently, the signal amplitude as a function of pressure has the same shape and position as the SNR curve.

Measurements of the CH_4 channel response to different CH_4 concentrations at the optimal pressure of 200 Torr verified the CH_4 channel linearity. The laser wavelength was locked to the center of the 6057.1 cm^{-1} absorption line. Four gas cylinders containing different calibrated CH_4 concentration levels were used to supply the sample gas. The results of measurements performed every 1 s are shown in Fig. 7(a). Same data averaged and plotted as a function of concentration from four certified CH_4 gas cylinders are shown in Fig. 7(b). These measurements were made for a dynamic range of only 100 because of the limited availability of calibrated gas samples. Previous CO_2 and NO experiments indicated that the linear dynamic range of a QEPAS-based sensor can cover at least 4 orders of

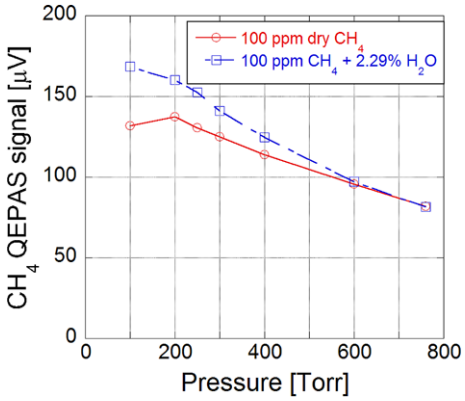

Fig. 8 Measured QEPAS signals for 100 ppm CH_4 in dry H_2 and H_2 with 2.29% H_2O vapor as a function of total gas pressure

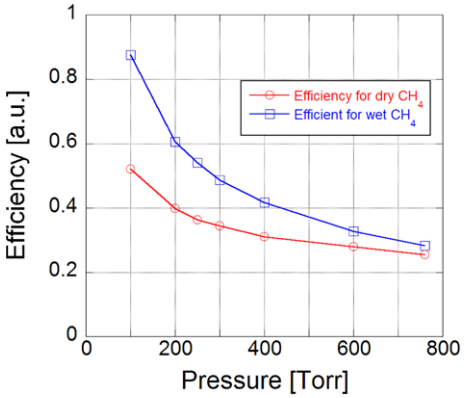

Fig. 9 Efficiency of the optical radiation-to-sound conversion $\varepsilon(p)$ as a function of total pressures for CH_4 in dry H_2 and H_2 with 2.29% H_2O vapor

magnitude [11] as the QTF is known to be a linear response transducer with a dynamic range of $>10^7$. The absolute detection sensitivity of the QEPAS sensor to CH_4 in dry H_2 was also evaluated. The scatter of consecutive measurements at a certain concentration level did not depend on the concentration. The noise level based on scatter data was 4.6 μV with $\Delta f = 0.785$ Hz. The calculated noise level was 4.8 μV based on (5) ($R = 56.4$ kΩ). This agreement confirms that no excess noise is introduced. This noise level results in a noise-equivalent (1σ) concentration of 3.2 ppm with a 1-s averaging time (0.785 Hz). Normalized to a 15.8-mW optical power and a 0.785-Hz detection bandwidth, the noise-equivalent absorption coefficient is 2.45×10^{-8} cm^{-1} W/$\sqrt{}$Hz. This coefficient is slightly lower when compared with the CH_4 detection sensitivity in dry N_2 (2.9×10^{-8} cm^{-1} W/$\sqrt{}$Hz).

5 CH_4 conversion efficiency in the presence of H_2O vapor

For trace methane in a nitrogen mixture, the observed QEPAS signal generated at a certain CH_4 concentration is much stronger in the presence of H_2O vapor as the water is an efficient catalyst for the vibrational energy transfer reactions in the gas phase. Hence, the influence of H_2O on overall QEPAS signal when using hydrogen as the carrier gas was investigated. First, 2.29% H_2O vapor was added to the 100-ppm dry CH_4 by means of a Nafion tube. The $2f$ peak values were recorded at different pressures and are shown in Fig. 8. For comparison, the QEPAS signals of the 100-ppm dry CH_4 are also plotted. The signal enhancement is not as high as in the case of using a nitrogen carrier [19]. At low pressures (<300 Torr), the enhancement factor is only ∼15%. With increasing pressure, the QEPAS signals from the dry and wet gases gradually overlap. However, the addition of water vapor strongly impacts the Q factor and R values of the QTF, as shown in Fig. 5 (solid lines). The Q factor decreases from an initial range of 30,000–50,000 to a final range of 27,500–37,500 and as a result, the R values increase from 53–86 kΩ to 70–95 kΩ, respectively.

Equation (1) was used to obtain the conversion efficiency $\varepsilon(p)$ as a function of pressure that is shown in Fig. 9. At pressures between 100 and 760 Torr, a higher total gas pressure does not help promote the V-T relaxation rate of CH_4. Instead, the conversion efficiency decreased towards higher pressures. The behavior of both $\varepsilon(p)$ values can be explained by the diffusion of the excited molecules to the QTF's prongs or the mR tube wall with subsequent V-T relaxation collisions. The mean diffusion path traveled by an excited CH_4 molecule was calculated in order to check if they are able to reach the tubes' wall within a modulation period $t = 1/f_0 = 30.5$ μs. The diffusion coefficient in the CH_4/H_2 mixture at $T = 297$ K and atmospheric pressure (P_{atm}) is $D_{12} = 0.721$ cm^2/s [22]. Using the 2D diffusion formula ($\sqrt{\langle l^2 \rangle} = \sqrt{4 D_{12} \frac{P_{\text{atm}}}{P} t}$) [19], the diffusion path is 260 μm at 100 Torr, which is comparable with the mR radius of 290 μm. At 760 Torr, a diffusion path of ∼100 μm is obtained. Taking into account the ∼100-μm diameter of the laser beam and the 300-μm gap between two prongs of QTF, excited CH_4 molecules are still able to reach the QTF's prongs and release their vibrational energy. Hence, we can conclude that the observed higher conversion efficiency at low-pressure CH_4/H_2 is most likely the result of diffusion. With increasing pressure, the diffusion effect decreases and the collision deexcitation process between CH_4 and H_2 molecules becomes gradually dominant. When considering H_2O influence, it was determined that the conversion efficiency $\varepsilon(p)$ induced by H_2O vapor is not a constant for different pressures but rather has a larger value at lower gas pressures. This can be explained by increased collisions between excited H_2O molecules and the mR tubes with the longer diffusion path, which further enhances the QEPAS signal.

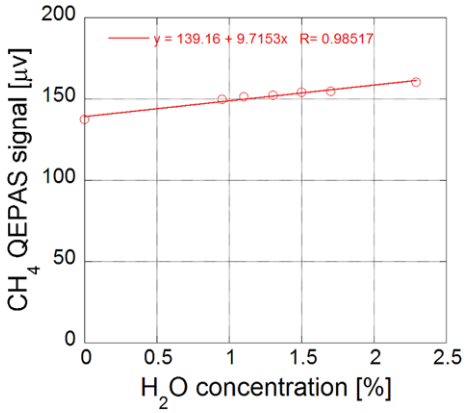

Fig. 10 QEPAS signal as a function of H_2O concentration in a CH_4/H_2 mixture with a linear fit

The influence of the different H_2O vapor concentrations on the QEPAS signal was measured at the optimal pressure of 200 Torr as shown in Fig. 10. A linear fit can be used for the experimental results in Fig. 10, based on the model reported in Ref. [19] as H_2O does not significantly promote vibrational deexcitation of CH_4 in H_2. Such a fit yields the relaxation time constant ${\tau_0}^{\mathrm{H}}P_0 = 23 \pm 1.7$ μs Torr, which describes V-T relaxation rate due to CH_4/H_2O collisions. The obtained value is 2.5 times slower than in wet nitrogen. The linear fit can be used as the correction curve to derive the actual CH_4 concentration value when H_2O vapor is present in a gas mixture.

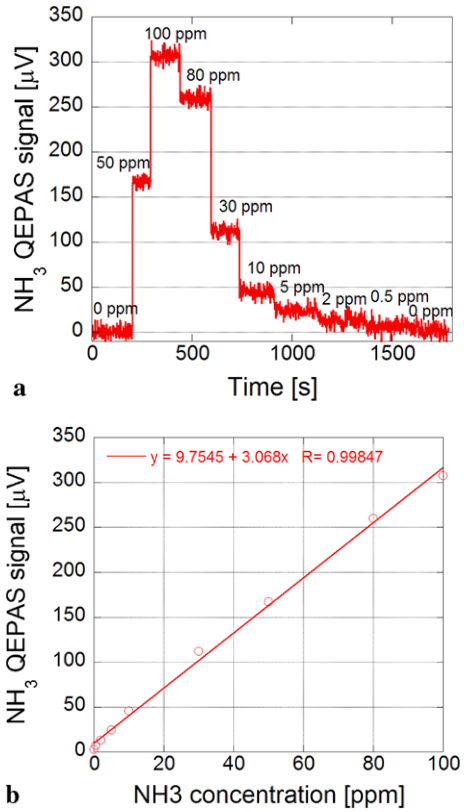

Fig. 11 (**a**) QEPAS signal acquired repetitively while the CH_4 concentration was varied by changing of the carrier gas flow using a standard gas generator. (**b**) Same data averaged and plotted as a function of the calibration of the standard gas generator

6 Optimization and sensitivity of the NH_3 detection channel

The NH_3 absorption line at 6528.76 cm^{-1} was selected as the target line for NH_3 detection based on data reported by Webber et al. [23]. An example of the QEPAS spectra acquired with 50 ppm NH_3 at 50 Torr and 760 Torr H_2 is shown in Fig. 3(b). The selected line merges with a weaker line at 6528.89 at pressures > 600 Torr. A similar optimization process of working gas pressure and wavelength modulation depth as was completed for CH_4 was carried out for the NH_3 channel. The results are shown in Fig. 4(b). Unlike CH_4 which detected at an optimal pressure of ~200 Torr, the optimal pressure for NH_3 detection is 50 Torr. Subsequently, the NH_3 QEPAS signal decreased towards higher pressures until the two discrete absorption lines start to merge at 600 Torr. Similar plots of the Q factor and R values as observed for a dry CH_4/H_2 mixture were obtained. Based on the data in Fig. 4(b) and R values calculated via (6), the SNR for the optimal laser current modulation amplitude was plotted in Fig. 6(b). The maximum SNR occurs at 50 Torr. However, the SNR has a second peak at pressures > 600 Torr regardless of the Q factor decrease. This enhancement results from an increase of the absorption coefficient due to the merging of two absorption lines, as shown in Fig. 3(b). Thus, we can operate the NH_3 channel at ambient atmospheric pressure with only a 1/4 loss of detection sensitivity.

The linearity and detection sensitivity of the NH_3 channel were evaluated by measuring its response to varying NH_3 concentrations in a 150 sccm H_2 flow. A gas standard generator (Kin-Tec) was employed to produce different NH_3 concentrations. The diode laser wavelength was locked to the center of the 6528.76 cm^{-1} NH_3 absorption line. The measurements were carried out at a pressure of 50 Torr. The results were recorded with a 1-s averaging time and are depicted in Fig. 11(a). Same data averaged as a function of the calibration of the standard gas generator are plotted in Fig. 11(b). At 50 Torr pressure, the measured R value is 47.6 Ω. With $\Delta f = 0.785$ Hz, the calculated noise level for NH_3 detection is 5.2 μV. The scatter of consecutive measurements (noise level) is 5.1 μV which is in good agreement with the predicted value. This noise level yields a noise-equivalent (1σ) concentration of 1.27 ppm with a 1-s averaging time (0.785 Hz). The noise-equivalent absorption coefficient is 9.1×10^{-9} cm^{-1} W/$\sqrt{}$Hz normal-

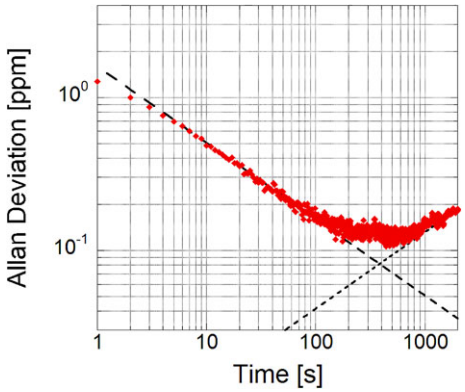

Fig. 12 Allan deviation as a function of the data averaging period. *Solid circles trace*: laser is locked to the NH_3 absorption line, data acquisition time 1 s. *Dashed line*: $1/\sqrt{t}$ slope. Dotted line: $\sqrt{t}$ slope

ized to a 50.2-mW optical power and a 0.785-Hz detection bandwidth, which is comparable to the value of 7.2×10^{-9} cm^{-1} $W/\sqrt{Hz}$ obtained in N_2.

The less distinct NH_3 linearity is due to the error introduced by the gas standard generator calibrated using N_2 and not H_2 as the carrier gas. Varying flow rates ranging from 20 to 500 sccm were measured for the two sensing channels. No excessive flow noise was observed. Due to the fast V-T relaxation rate of NH_3 [20], the influence of water vapor as a V-T relaxer can be neglected.

In order to characterize long-term drifts and establish signal averaging limits, the results of the Allan deviation $\sqrt{\langle \sigma_A^2 \rangle}$ in terms of ammonia concentration for the NH_3 channel are presented in Fig. 12. For this analysis, the laser frequency was locked to the NH_3 absorption line at 6528.76 cm^{-1}, and pure carrier gas H_2 was introduced into the ADM. The Allan deviation at the beginning closely follows a $1/\sqrt{t}$ dependence, which indicates that white Johnson noise of the QTF remains the dominant source of noise for time sequences of 1 to 200 s [24]. However, the Allan deviation experiences a sensitivity drift following a $\sqrt{t}$ dependence when averaging exceed 600 s. Thus a stability period of 200–600 s and an optimal detection sensitivity of 100–150 ppb are determined. Since the same ADM and carrier gas are used for the CH_4 channel, the minimum Allan deviation of CH_4 is shifted only in the vertical direction. Hence, the CH_4 exhibits the same stability period as the NH_3 channel.

7 Conclusions

An outline for the detection of residuals CH_4 and NH_3 in impure hydrogen gas using QEPAS has been presented. Although the enhancing factor of a non-matched mR is lower than that of a matched mR, the non-matched mR is better suited for detection of impurities in hydrogen. In fact, in hydrogen, the QTF has a relatively high Q factor. The reduction of the QEPAS signal associated with a non-matched mR is compensated by the high Q factor of the QTF when in a hydrogen carrier gas environment (i.e. with a Q factor ranging from a $Q = 55{,}000$ at 50 Torr to a $Q = 30{,}000$ at atmospheric pressure) compared to the Q in nitrogen (where the Q factor ranges from a 30,000 in 50 Torr to 2000 at atmospheric pressure). As a result, the sensitivity of the non-matched QEPAS configuration employed in H_2 can achieve comparable or increased detection sensitivity as an optimal QEPAS sensor configuration for N_2 with the additional benefit of a shorter mR length, which facilitates optical alignment of the optical coupling scheme from diode laser to ADM. The addition of H_2O does not significantly promote vibrational deexcitation of CH_4 in H_2, although it is efficient in the case of a CH_4/N_2 mixture. In the presence of high H_2O vapor concentrations (>2000 ppmv), a correction to the measured CH_4 concentration is necessary by monitoring the H_2O content. In addition, the optimal detection pressures for CH_4 and NH_3 do not coincide. When two gases were measured simultaneously in one sample gas, a pressure of 100 Torr was used. In this case each channel loses ~8% SNRs. The QEPAS response is directly proportional to the laser power. Therefore the noise-equivalent concentration limits can be much lower if either a higher power diode laser source or fiber-amplified diode laser source is used. In addition, the system allows useful data averaging for long time periods up to 200 s to obtain lower background noise level and improved detection sensitivity.

For a static gas measurement, it was found that the optical alignment of epoxied components in the QEPAS ADM is vulnerable to sudden large pressure changes. This issue can be solved by using solder processing, instead of epoxy processing, in mounting all ADM parts in the next generation of the ADM design. The CEU for the two target analytes can be preprogrammed to be capable of controlling the acquisition of up to 10 sets of QEPAS based sensor parameters. Each set includes the selection of the diode laser, reference cell, laser current and temperature settings, modulation depth and regulation parameters. Based on the function of CEU and a 4×4 MEM optical switch, the current two-gas sensor design can be adapted to a multi-gas sensor by adding more commercially available CW TEC DFB diode lasers. The CEU can be programmed to loop through desired diode lasers in an autonomous mode, which leads a diode laser based sensor design that is compact, user-friendly and cost-effective.

Acknowledgements The Rice University group acknowledges financial support from a National Science Foundation ERC MIRTHE award and a Grant C-0586 from the Welch Foundation. Significant funding was also provided by the Department of Energy (DOE) National Nuclear Security Administration (NNSA) Readiness Campaign (NA-123).

References

1. A.A. Kosterev, F.K. Tittel, D.V. Serebryakov, A.L. Malinovsky, I.V. Morozov, Rev. Sci. Instrum. **76**, 043105 (2005)
2. A.A. Kosterev, Y.A. Bakhirkin, R.F. Curl, F.K. Tittel, Opt. Lett. **27**, 1902 (2002)
3. L. Dong, A.A. Kosterev, D. Thomazy, F.K. Tittel, Appl. Phys. B **100**, 627 (2010)
4. A. Miklos, P. Hess, Z. Bozoki, Rev. Sci. Instrum. **72**, 1937 (2001)
5. D.V. Serebryakov, I.V. Morozov, A.A. Kosterev, V.S. Letokhov, Quantum Electron. **40**, 167 (2010)
6. A.A. Kosterev, F.K. Tittel, Appl. Opt. **43**, 6213 (2004)
7. L. Dong, A.A. Kosterev, D. Thomazy, F.K. Tittel, Proc. SPIE **7945**, 50R-1 (2011)
8. D. Weidmann, A. A Kosterev, F. K Tittel, N. Ryan, D. McDonald, Opt. Lett. **29**, 1837 (2004)
9. A.A. Kosterev, L. Dong, D. Thomazy, F.K. Tittel, S. Overby, Appl. Phys. B, Lasers Opt. **101**, 649 (2010)
10. S. Schilt, Anatoliy A. Kosterev, Frank K. Tittel, Appl. Phys. B **95**, 813 (2009)
11. L. Dong, V. Spagnolo, R. Lewicki, F.K. Tittel, Opt. Express **19**, 24037 (2011)
12. V. Spagnolo, A.A. Kosterev, L. Dong, R. Lewicki, F.K. Tittel, Appl. Phys. B, Lasers Opt. **100**, 125 (2010)
13. A. A Kosterev, Y.A. Bakhirkin, F.K. Tittel, Appl. Phys. B **80**, 133 (2005)
14. R. Lewicki, A.A. Kosterev, D.M. Thomazy, T.H. Risby, S. Solga, T.B. Schwartz, F.K. Tittel, Proc. SPIE **7945**, 50K-2 (2011)
15. A.K. Ngai, S.T. Persijni, D. Lindsay, Anatoliy A. Kosterev, P. Gross, C.J. Lee, C.M. Cristescu, Frank K. Tittel, K.J. Boller, F.J. Harren, Appl. Phys. B **89**, 123 (2007)
16. M. Horstjann, Y. A Bakhirkin, A.A. Kosterev, R.F. Curl, F.K. Tittel, C.M. Wong, C.J. Hill, R.Q. Yang, Appl. Phys. B **79**, 799 (2004)
17. A.A. Kosterev, P.R. Buerki, L. Dong, M. Reed, T. Day, F.K. Tittel, Appl. Phys. B, Lasers Opt. **100**, 173 (2010)
18. R.C. Weast, M.J. Astle, *CRC Handbook of Chemistry and Physics*, 61st edn. (CRC Press, Boca Raton, 1980–1981)
19. A.A. Kosterev, Y.A. Bakhirkin, F.K. Tittel, S. Mcwhorter, B. Ashcraft, Appl. Phys. B, Lasers Opt. **92**, 103 (2008)
20. T.L. Cottrell, J.C. McCoubrey, *Molecular Energy Transfer in Gases* (Butterworths, London, 1961)
21. A.A. Kosterev, T.S. Mosely, F.K. Tittel, Appl. Phys. B, Lasers Opt. **85**, 295 (2006)
22. C.R. Wilke, C.Y. Lee, Ind. Eng. Chem. **47**, 1253 (1955)
23. M.E. Webber, M. Pushkarsky, C.K.N. Patel, Appl. Opt. **42**, 2119 (2003)
24. P. Werle, Appl. Phys. B **102**, 313 (2011)